

Received October 18, 2021, accepted October 26, 2021, date of publication November 2, 2021, date of current version November 11, 2021.

Digital Object Identifier 10.1109/ACCESS.2021.3125053

# Design of Dualband Bandpass High-Temperature Superconducting Filter With Group Delay Equalization

KAI YANG<sup>1,2</sup>, MINGYANG SU<sup>3</sup>, AND PENG CHEN<sup>1,2</sup>

<sup>1</sup>School of Aeronautics and Astronautics, University of Electronic Science and Technology of China, Chengdu 611731, China

<sup>2</sup>Aircraft Swarm Intelligent Sensing and Cooperative Control Key Laboratory of Sichuan Province, Chengdu 611731, China

<sup>3</sup>Tuowei Electronics Technology (Shanghai) Company Ltd., Shanghai 201101, China

Corresponding author: Peng Chen (chenp@uestc.edu.cn)

This work was supported in part by the National Natural Science Foundation of China under Grant 61601088, in part by the Sichuan Provincial Science and Technology Plan under Grant 2021YJ0090, in part by the Chengdu Science and Technology Program under Grant 2019-YF08-00248-GX, and in part by the Fundamental Research Funds for the Central Universities under Grant ZYGX2019J085.

**ABSTRACT** A novel dualband high-temperature superconducting (HTS) bandpass filter is proposed with group delay equalization for 5G emergency communication receivers with N41 and N79 bands in this paper. The dual-folded stub-loaded stepped impedance resonator (DSLSIR) is applied to realize dualband performance. The proposed DSLSIR has miniaturized circuit size and more design freedom to independently adjust the two designed center frequencies, comparing with other reported DSLSIRs. Two cross-coupling transmission lines are added at the top and bottom parts of the cascaded sixth-order filter with DSLSIRs to flatten the group delay of the passband at both bands. A dualband bandpass HTS filter etched on the YBCO superconducting material is fabricated to verify the proposed design method. The measurement is actualized at the temperature of 77 K to make YBCO microstrip lines perform superconducting features. The results show that the first center frequency is 2.595 GHz with 6.2% bandwidth for N41 band and 0.3 dB insertion loss while the second center frequency is 4.85 GHz with 2% bandwidth for N79 band and 0.4 dB insertion loss. Meanwhile, the group delays at the N41 and N79 bands keep 2 ns fluctuations in the 60% passband. The agreement between the measured and simulated results indicates that the proposed dualband bandpass HTS filter with low insertion loss, sharp roll-off skirt and flat group delay is a promising candidate for emergency communication receiver.


**INDEX TERMS** Dualband bandpass filter, group delay equalization, high temperature superconductor, linear phase, stub-loaded stepped-impedance resonator (SLSIR).

## I. INTRODUCTION

Emergency communications in catastrophic situations, such as forest fires, floods, landslides, mudslides and earthquakes, have crucial requirements of the radio frequency receiver on the sensitivity and roll-off rate for better signal covering range. It is believed that the receiver based on the planar filter with HTS material has the highest sensitivity except for quantum sensing receivers because of the extremely low surface resistance of the HTS material, which is 1000 times less than conventional metals, such as annualized copper and silver, at Giga-Hertz range [1]–[3]. The HTS bandpass filter

merits of very low insertion loss, very high Q-factor, very narrow bandwidth, very high out-of-band rejection and an extremely steep skirt slope [2]. With the increasing development of multi-service wireless communication requirements, the multi-band bandpass HTS filters have also been highly demanded for emergency communication receivers of multi-band standards and several published papers are focusing on this field in recent years [4]–[11].

The stub-loaded folded microstrip-line resonators are employed to design an eight-pole dualband HTS bandpass filter with dualband bandwidths controlling [4]. The asymmetric trisection stepped-impedance resonator [5] and the embedded stub-loaded resonator [6] have been used to design tri-band HTS bandpass filter, respectively.

The associate editor coordinating the review of this manuscript and approving it for publication was Mauro Fadda .

Conclusively, most of the multi-band bandpass HTS filters are based on the modified stub-loaded resonator and modified stepped-impedance resonator. Both of them can be applied to adjust working bandwidths and transmission zeros separately of the designed bands simultaneously [7]–[11]. All of these multi-band bandpass HTS filters as mentioned earlier have low insertion loss and sharp roll-off skirts. However, the resonator should be further improved to increase design freedom to simultaneously control the passband return loss and out-of-band rejection characteristics.

As an index of the signal phase distortion, the group delay is another crucial factor to the emergency communication receiver. The flat group delay of a bandpass filter is highly demanded for a high-capacity communication receiver to realize the good linear phase response over the center of the passband for a lower bit error ratio (BER) [12]. Although some works have been reported about the single bandpass HTS filter with linear-phase design [12]–[14], there is no report of the dualband passband HTS filter with dualband group delay equalization.

In this paper, a dualband bandpass HTS filter designed for N41 (2515–2675 MHz, 160 MHz bandwidth) band and N79 (4800–4900 MHz, 100 MHz bandwidth) band with dualband group delay equalization is presented using a novel DSLSIR. Two cross-coupling lines are applied to smooth the group delay for better linearity of the whole filter. The resonant characteristics of the dualband DSLSIR are investigated and the parameter studies of the dualband DSLSIR and external quality factor are given to guide the filter design. An experiment based on the proposed design method is implemented and the measured results prove its effectiveness. This is the first reported dualband bandpass HTS filter with dualband group delay equalization to the best of our knowledge.

## II. IMPLEMENTATION OF THE HTS FILTER

### A. RESONANCE ANALYSIS OF DSLSIR

The equivalent circuit model of the proposed DSLSIR is displayed in Fig. 1(a), which consists of two parts: the symmetrical SIR part and the open stub part. The characteristic impedances and the corresponding electrical lengths are represented as  $Z_1, Z_2, Z_3$  and  $\theta_1, \theta_2, \theta_3$ , respectively. The length of the symmetrical SIR is  $\lambda_1/2$  as initial while the length of the open stub is  $\lambda_2/2$  as initial, where  $\lambda_1$  and  $\lambda_2$  are the wavelengths of the designed center frequency  $f_1$  and  $f_2$  of N41 and N79 bands, respectively. The equivalent circuit model of the traditional SIR is also shown in Fig. 1(b) for comparison.

Considering the symmetry of the equivalent circuit, the odd-mode and even-mode analyses are used to calculate the resonance characteristic of the proposed DSLSIR. An electrical wall can be added along the T-T' plane and the odd-mode circuit is shown in Fig. 1(c). Meanwhile, a magnetic wall can be added along the T-T' plane and the even-mode circuit is shown in Fig. 1(d). The proposed DSLSIR has the same behavior as the traditional stub-loaded SIR, which has been discussed in [15]. The theoretical analysis is duplicated

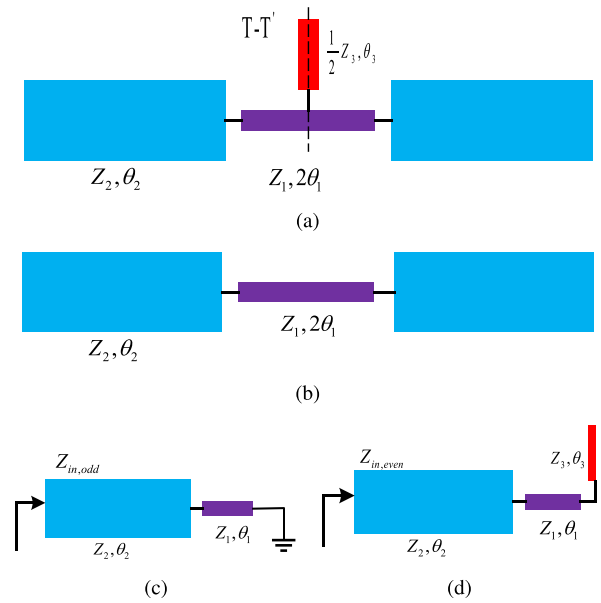


**FIGURE 1. Transmission line equivalent circuit models: (a) proposed SLSIR (lines unfolded); (b) traditional SIR; (c) odd model of DSLSIR; (d) even model of DSLSIR.**

here to help the readers understand the transform necessity from the traditional SLSIR to the proposed DSLSIR.

The input admittance of the odd mode is [15]

$$Y_{in,odd} = \frac{1}{jZ_2} \cdot \frac{Z_2 - Z_1 \tan(\theta_1) \tan(\theta_2)}{Z_1 \tan(\theta_1) + Z_2 \tan(\theta_2)} \quad (1)$$

The odd-mode resonance condition is achieved when  $Y_{in,odd}$  is zero, that is,

$$Z_2 - Z_1 \tan(\theta_1) \tan(\theta_2) = 0 \quad (2)$$

Similarly, input impedance of the even mode is [15]

$$Y_{in,even} = \frac{jZ_2A + jZ_1 \tan(\theta_2)B}{Z_1Z_2B - Z_2^2 \tan(\theta_2)A} \quad (3)$$

where

$$A = Z_1 \tan(\theta_3)A + Z_3 \tan(\theta_1) \quad (4)$$

$$B = Z_3 - Z_1 \tan(\theta_1) \tan(\theta_3) \quad (5)$$

The even-mode resonance condition is achieved when  $Y_{in,even}$  is zero, that is,

$$jZ_2A + jZ_1 \tan(\theta_2)B = 0 \quad (6)$$

It can be further reduced as

$$\tan(\theta_1) \tan(\theta_2) \tan(\theta_3) = \frac{Z_2 Z_3}{Z_1 Z_1} \tan(\theta_1) + \frac{Z_3}{Z_1} \tan(\theta_2) + \frac{Z_2}{Z_1} \tan(\theta_3) \quad (7)$$

The first odd mode resonance frequency  $f_{o1}$  and the first even mode resonance frequency  $f_{e1}$  could be selected to design a dualband resonator. Practically, the widths of these lines are determined firstly to meet the requirement of the current capacity and then the lengths of these lines are optimized

by a full-wave simulation software since the cross-coupling effect could change the calculation results. However, the calculated lengths are still needed for a better initial guess, which is essential to accelerate the optimization process. It is worthy to note that the open stub part is irrelevant to the odd resonance while the SIR part is related to both the odd mode and even mode simultaneously. As a result,  $Z_1$ ,  $Z_2$ ,  $\theta_1$  and  $\theta_2$  could be firstly designed to meet the even resonance condition. When  $Z_1$ ,  $Z_2$ ,  $\theta_1$  and  $\theta_2$  are determined,  $Z_3$  and  $\theta_3$  could be individually confirmed to meet the odd resonance condition. As the existence of the open stub, the two resonance frequencies of the proposed DSLSIR can be determined independently, which brings in more design convenience of the required dualband resonator comprising with the traditional SIR.

In order to reduce the circuit size for superconducting film realization, all the stubs of the DSLSIR need to be folded. There are two main concerns. The first one is that the SIR with low-high-low impedance transmission lines is used to move the odd mode harmonic resonance far away from the two designed frequencies to obtain good rejection between  $f_1$  and  $f_2$ . Also, the low impedance stub with broader width at the end of the SIR is used to reserve space for further cross-coupling energy adjustment, which is the key to realize the group delay control. The second one is that the SIR and the open stub should extend inversely to ensure the final filter have the ability to adjust the coupling coefficient of the adjacent resonator at  $f_1$  and  $f_2$  independently. The final designed dualband DSLSIR is illustrated in Fig. 2.

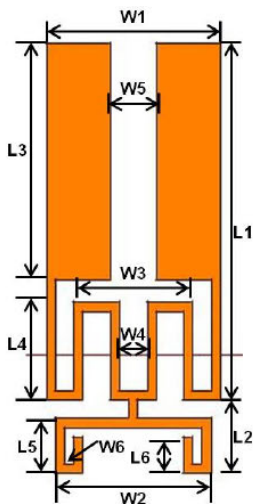


FIGURE 2. The structure of the proposed DSLSIR.

The electrical distribution simulation results of the proposed DSLSIR at  $f_1$  and  $f_2$  are also given in Fig. 3. Almost all the energy at  $f_1$  distributes at the SIR part while the energy at  $f_2$  distributes at both the SIR part and the open stub. It is clear that the lower resonant frequency is mainly controlled by the SIR part, just as the suggestion of the theoretical analysis results.

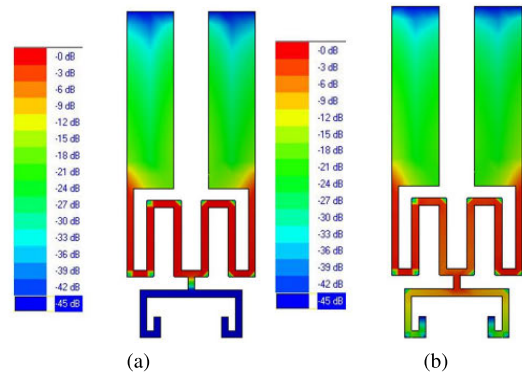


FIGURE 3. The Electrical distribution simulation of the proposed DSLSIR: (a) at 2.595 GHz; (b) at 4.850 GHz.

The parameter study results of the proposed DSLSIR are plotted in Fig. 4. When  $W_2$  is fixed at 1.7 mm, the higher resonant frequency is only determined by the length of  $L_2$  while the lower resonant frequency remains unchanged. With the increase of the length  $L_2$ , the higher resonant frequency decreases from 5.5 GHz to 4.4 GHz, as shown in Fig. 4(a). The adjustment of  $L_6$  has a similar result as displayed in Fig. 4(b). It is evident that the higher resonant frequency could be independently controlled by the open stub, which agrees with the theoretical analysis results mentioned earlier. When  $W_1$  is fixed at 1.9 mm, the increase of  $L_1$  could make the higher and lower resonant frequency decrease with almost the same speed as shown in Fig. 4(c). However, the increase of  $L_4$  could also make the higher and lower resonant frequency decrease but the higher resonant frequency decreases faster than the lower one as displayed in Fig. 4(d). The resonant frequencies are more sensitive to the length  $L_1$ . As a result, the length  $L_1$  and  $L_4$  affect the higher and lower resonant frequencies while the length  $L_2$  and  $L_6$  only affect the higher resonant frequency.

The presented dualband DSLSIR design method is summarized as follows.

- 1) Calculate the initial microstrip line lengths of the two designed resonant frequencies with the given dielectric coefficient and substrate height.
- 2) Layout the structure of the DSLSIR as Fig. 2, where the width of the folded SIR part and the width of the folded open stub part should have space to be adjusted independently for further coupling coefficient control between neighboring dualband resonators.
- 3) Adjust the length  $L_1$  and  $L_4$  to ensure the lower resonant frequency be the correct position.
- 4) Regulate the length  $L_2$  and  $L_6$  to ensure the higher resonant frequency be the right position.
- 5) Optimize all the geometrical parameters in a full-wave simulation software to ensure both the higher and lower resonant be the same as requirements.

The lanthanum aluminate ( $\text{LaAlO}_3$ ) substrate with the dielectric coefficient of 24.1 and height of 0.5 mm is used in this paper for minimized circuit size. The S-parameter simulation result of the proposed DSLSIR is displayed in Fig. 5.

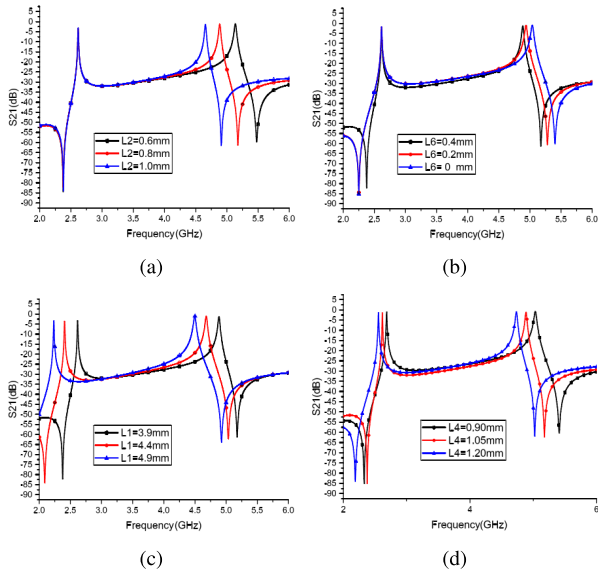


FIGURE 4. The parameter study results, the simulated  $S_{21}$  varies with: (a)  $L_2$ ; (b)  $L_6$ ; (c)  $L_1$ ; (d)  $L_4$ .

The lower resonant frequency is at 4.595 GHz and the higher one is at 4.850 GHz and there is no spurious harmonic frequency between the designed two bands. The first spurious harmonic frequency appears approximately at 9.90 GHz and it is far away from the higher frequency, which is favorable for the out-of-band rejection improvement.

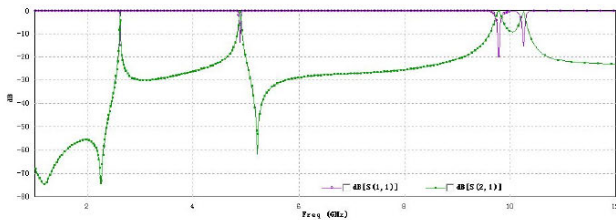


FIGURE 5. The simulation result of the proposed DSLSIR.

### B. DUALBAND COUPLING MATRIX DESIGN

For demonstration, the proposed DSLSIR is employed to design a dualband bandpass HTS filter at N41 and N79 bands for 5G emergency communication receiver. The even-mode resonant frequency is designed at 2.595 GHz and the odd-mode resonant frequency is designed at 4.850 GHz. The coupling matrix of the two bands are parallel, just as shown in Fig. 6, since they have different center frequencies and bandwidths.

The coupling coefficients are calculated by the sixth order Chebyshev low-pass filter prototype with 0.01 dB ripple [16]:  $g_0 = 1.000$ ,  $g_1 = 0.7813$ ,  $g_2 = 1.3600$ ,  $g_3 = 1.6896$ ,  $g_4 = 1.5350$ ,  $g_5 = 1.4970$ ,  $g_6 = 0.7098$  and  $g_7 = 1.1007$ .

The normalized coupling coefficients are written as [17]

$$m_{i,i+1} = \frac{1}{\sqrt{g_i g_{i+1}}} \quad (8)$$

where  $i = 0, 1, \dots, 7$  represents the index of the resonator.

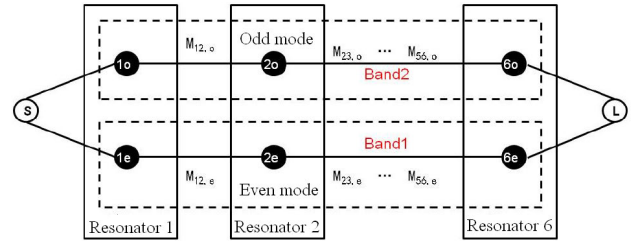


FIGURE 6. The coupling structure of the dualband HTS filter.

And the coupling coefficients are [17]

$$M_{i,i+1} = m_{i,i+1} \text{FBW} \quad (9)$$

where FBW is the fractional bandwidth which is

$$\text{FBW} = \frac{f_h - f_l}{f_0} \quad (10)$$

where  $f_h$ ,  $f_l$  and  $f_0$  represent the upper cut-off frequency, the lower cut-off frequency and the center frequency of every band, respectively.

The external quality factor between the input port and the first resonator  $Q_{ei}$  and the external quality factor between the output port and the last resonator  $Q_{eo}$  can be calculated by [17]

$$Q_{ei} = \frac{g_0 g_1}{\text{FBW}} \quad (11)$$

$$Q_{eo} = \frac{g_6 g_7}{\text{FBW}} \quad (12)$$

The final coupling coefficients at the two designed bands are illustrated in table 1.

TABLE 1. Coupling coefficients calculation results.

$f_0/\text{GHz}$	$Q_{ei}$	$M_{12}$	$M_{23}$	$M_{34}$	$M_{45}$	$M_{56}$	$Q_{eo}$
2.595	12.672	0.0598	0.0407	0.0383	0.0407	0.0598	12.671
4.850	37.893	0.0200	0.0136	0.0128	0.0136	0.0200	37.891

### C. COUPLING COEFFICIENT EXTRACT

The dualband coupling coefficient extract circuit is shown in Fig. 7, where the gap  $s$  mainly controls the coupling coefficient of N41 while the gap  $d$  mainly controls the coupling coefficient of N79. The coupling coefficient can be extracted by the two peaks of the S-parameter simulation results of the two neighboring resonators, which is given as [17]

$$M = \frac{f_{p2}^2 - f_{p1}^2}{f_{p2}^2 + f_{p1}^2} \quad (13)$$

where  $f_{p2}$  and  $f_{p1}$  are the higher and lower peak resonant frequencies of the coupled resonators as illustrated in Fig. 7, respectively.

The simulated relationships between the coupling coefficient  $M$  and the two gaps are shown in Fig. 8, where “Band1” and “Band2” represent N41 and N79 bands respectively.

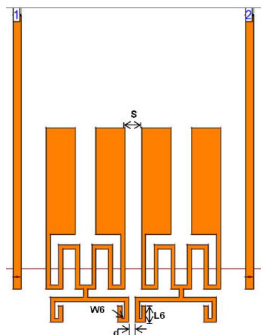


FIGURE 7. The dualband coupling coefficient extract simulation circuit.

As resonance analysis indicates, the coupling between the SIRs could affect both bands while the coupling between the open stubs only affects the N79 band. When  $d$  keeps constant and  $s$  increases, the coupling coefficients of the two bands monotonously decrease. Since the gap  $s$  has global effects, it should be determined by iterative optimization to make both the designed coupling coefficients at two bands are satisfied well.

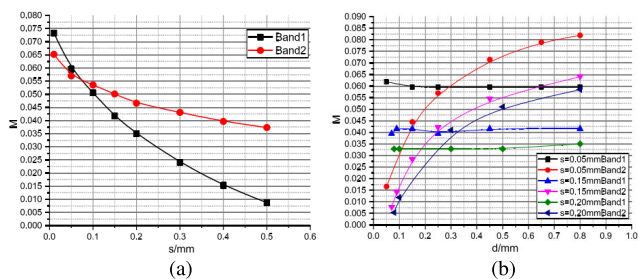


FIGURE 8. The coupling coefficient  $M$  changes as: (a) the gap  $s$ ; (b) the gap  $d$ .

The final calculated initial values of the coupling gaps are shown in table 2.

TABLE 2. The initial value of the calculated coupling gaps.

Resonator	1-2	2-3	3-4	4-5	5-6
$s/mm$	0.05	0.15	0.20	0.15	0.05
$d/mm$	0.06	0.08	0.12	0.08	0.06

D. EXTERNAL QUALITY FACTOR EXTRACT

Since the external quality factors are different at the two designed bands, the dual-feed external coupling structure which uses two feed tapped lines connecting to the SIR part and the open stub part respectively are demanded, just as depicted in Fig. 9. Each feed line has two design freedom, i.e., the height of the line,  $h_1$  or  $h_2$ , and the length of the line,  $t$  or  $h_3$ . As a result, there are four design freedom to adjust the dual external quality factor, which can be derived by the

group delay simulation result [6]:

$$Q_e = \frac{\omega_0}{\Delta\omega_{\pm 90^\circ}} \tag{14}$$

where  $\omega_0$  is the center angular frequency and  $\omega_{\pm 90^\circ}$  is the angular frequency offset the center frequency with  $\pm 90^\circ$  phase difference at resonant condition.

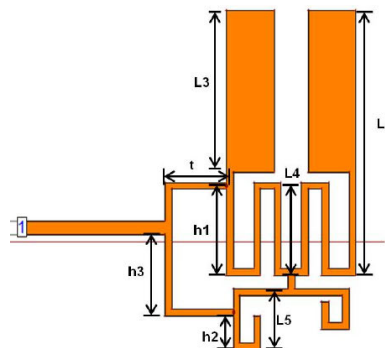


FIGURE 9. The external quality factor simulation circuit.

The parameter study of both  $Q_{e1}$  and  $Q_{e2}$  is shown in Fig. 10. As shown in Fig. 10(a), the height  $h_1$  affects both  $Q_{e1}$  and  $Q_{e2}$  simultaneously when  $h_3 = 1.3$  mm and  $h_2 = 0.5$  mm. When the height  $h_1$  increases,  $Q_{e1}$  decreases to 16.1 firstly and then increases continuously while  $Q_{e2}$  performs inversely. However,  $Q_{e1}$  changes within the small range while  $Q_{e2}$  decreases from 110 to 40 when  $h_2$  increases from 0.15 mm to 0.8 mm, on conditions of  $h_1 = 1.2$  mm and  $h_3 = 1.2$  mm, shown in Fig. 10(b). Fig. 10(c) and Fig. 10(d) indicate that the parameters  $h_3$  and  $t$  affect  $Q_{e1}$  and  $Q_{e2}$ . As a result,  $L_3$ ,  $L_4$  and  $L_5$  also should be optimized to obtain the demanded  $Q_{e1}$  and  $Q_{e2}$  simultaneously.

E. CROSS-COUPLING LINE DESIGN

The group delay represents the signal transit time through the filter as a function of frequency and is a measure of phase distortion. The flat group delay is always required in the filter’s passband to reduce the BER of the signal receiver. For the single-band filter, the cross-coupling line is often used to introduce transmission zeros in the real axis of the complex  $s$ -plane, which makes the filter work on the so-called “self-equalization” situation. Compared with the external-equalization with additional phase equalizer and circulator, the self-equalization merits of circuit miniaturization.

The cross-coupling quantity to realize the self-equalization could be calculated by [18]

$$k_{i,i+4} = \frac{FBW \cdot J_i}{g_i} \tag{15}$$

where  $J_i$  is

$$J_i = \begin{cases} \sqrt{1+h^2} + h, & i \text{ is odd} \\ \frac{1}{\sqrt{1+h^2} + h}, & i \text{ is even} \end{cases} \tag{16}$$

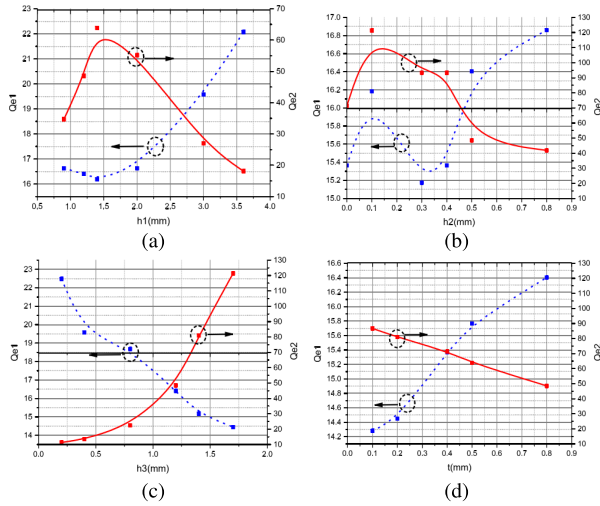


FIGURE 10. The simulated external quality factors  $Q_{e1}$  and  $Q_{e2}$  vary with: (a)  $h_1$ ; (b)  $h_2$ ; (c)  $h_3$ ; (d)  $t$ .

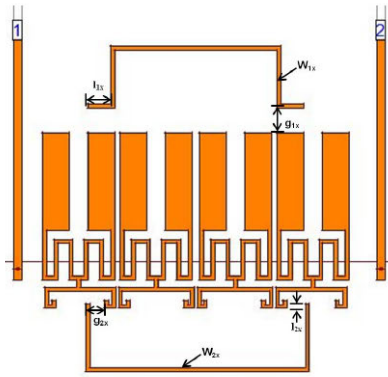


FIGURE 11. The coupling line simulation circuit.

where  $h = \sqrt{IL - 1}/f(x)$ ,  $IL$  and  $f(x)$  represent insertion loss in the passband and rational function of the filter, respectively.

In practical microstrip line filter design, the four resonator modules, also called as quadruplet, could produce complex transmission zeros in the complex  $s$ -plane to realized flat group delay performance on condition that the cross-coupling element is the same type as the main line coupling elements, i.e., all inductive or all capacitive.

In order to ensure the proposed HTS filter performs linear phase at the two designed bands, two cross-coupling lines are added to the SIR part and the open stub part to adjust the N41 and N79 bands, respectively, as depicted in Fig. 11. The width of the cross-coupling line should be small to avoid the coupling effect between the cross-coupling line and the second and third resonator. The final optimized parameters of the two cross-coupling lines are:  $W_{1x} = 0.1$ ,  $W_{2x} = 0.1$ ,  $g_{1x} = 0.66$ ,  $g_{2x} = 0.32$ ,  $l_{1x} = 0.60$  and  $l_{2x} = 0.10$  (Units: mm).

The group delay simulation results with/without the cross-coupling line are comprised in Fig. 12. The group delays

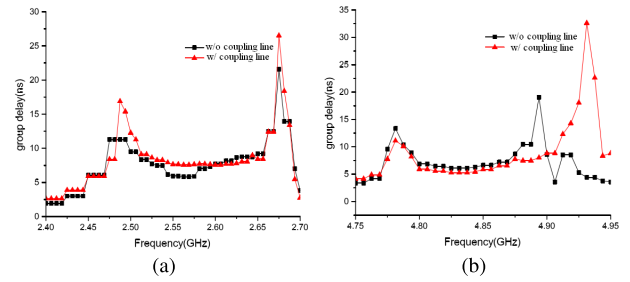


FIGURE 12. The group delay simulation results with/without cross-coupling line: (a) at 2.595 GHz; (b) at 4.850 GHz.

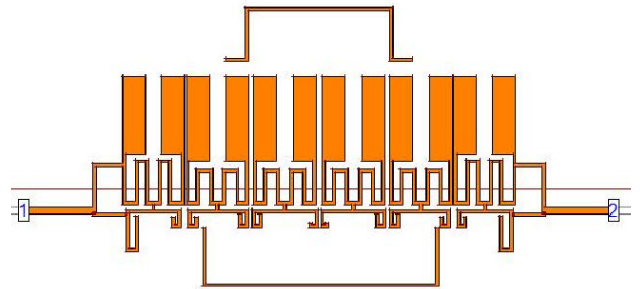


FIGURE 13. The whole dualband bandpass HTS filter structure.

fluctuate less than 1 ns in the 60% passband at 2.595 GHz and 4.850 GHz and the cross-coupling line could improve the group delay of the upper cut-off side-band at the N79 band. Regrettably, the upper cross-coupling line has a more negligible effect of improving the group delay fluctuation of the upper cut-off side-band at the N41 band although it actually flats the group delay in the passband.

### F. DUALBAND FILTER DESIGN

The final structure of the presented dualband bandpass HTS filter is shown in Fig. 13. Meanwhile, the electrical distribution simulation results of the quasi-TEM mode are given in Fig. 14. It can be concluded that the electrical energy main gathers the SIR part at 2.595 GHz and the open stub part at 4.850 GHz, respectively.

The comparison between the proposed dualband bandpass filter based on HTS film and common copper is shown in Fig. 15. It is evident that the HTS filter has the merits of better out-of-band rejection, lower insertion loss and sharper roll-off skirts, which has the property to increase the signal receiving range when it is applied for emergency communication.

### III. FABRICATION AND MEASUREMENT

The proposed dualband bandpass HTS filter is fabricated on the lanthanum aluminate substrate and double-side yttrium barium copper oxide (YBCO) films, which are with height of 500 nm. The surface of the YBCO film coats 300 nm gold for oxidation resistance protection and the circuit is etched by the ion beam etching method. The fabricated HTS filter

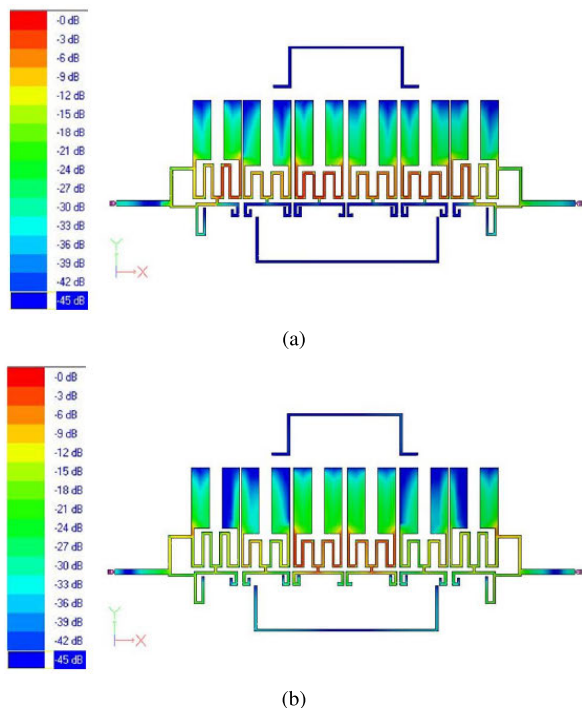


FIGURE 14. The electrical distribution simulation results: (a) at 2.595 GHz; (b) at 4.850 GHz.

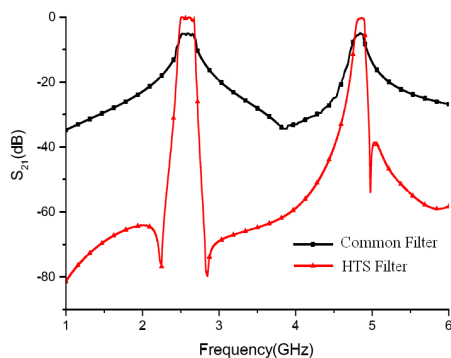


FIGURE 15. The simulation results comparison of the common copper filter and HTS filter.

is shown in Fig. 16 and it has the size of 21 mm × 9.5 mm. A copper shielded box is used for packaging the HTS filter for measuring convenience.

The proposed dualband bandpass HTS filter is measured by the Ceyear AV3672C vector network analyzer and the results are displayed in Fig. 17. The first band is at 2.51-2.67 GHz with 160 MHz bandwidth while the second band is at 4.81-4.91 GHz with 100 MHz. The first band has 0.3 dB insertion loss, 20.5 dB return loss and maximal 80 dB rejection off 100 MHz of the upper sideband while the second band has 0.4 dB insertion loss, 10.2 dB return loss and 35 dB rejection off 40 MHz of the upper sideband. There are two deviations in comparison with the simulation results. The first deviation is the insertion loss at both bands increase 0.3 dB while the second deviation is the passband deflects on the high side of 10 MHz. Both of the two deviations could have

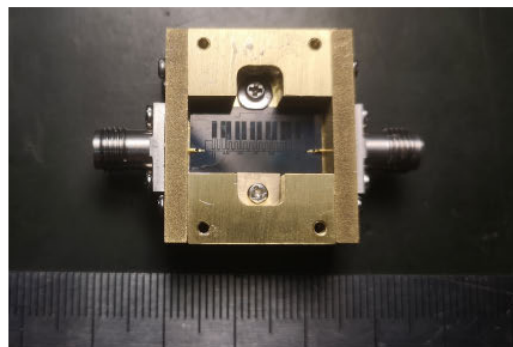


FIGURE 16. Photograph of the fabricated dualband bandpass HTS filter circuit.

been resulted from the machining tolerance, the uniformity of the YBCO film and the connection mismatch of the coaxial connectors and the filter substrate.

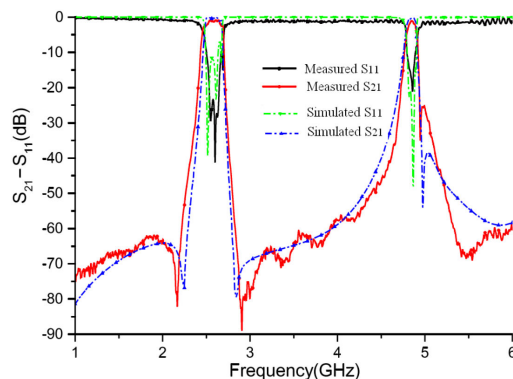


FIGURE 17. The measured S-parameter results of the dualband bandpass HTS filter.

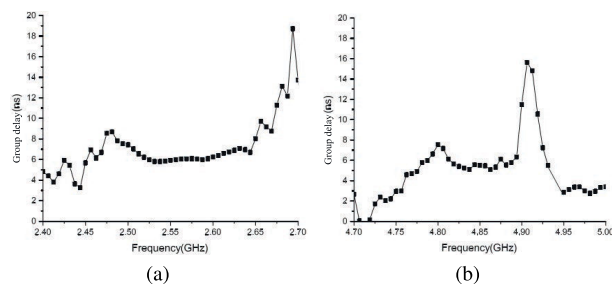


FIGURE 18. The group delay measured results of the dualband bandpass HTS filter: (a) at 2.595 GHz; (b) at 4.850 GHz.

The measured group delay results of the proposed dualband bandpass HTS filter are shown in Fig. 18. Interestingly, the worst group delay at the higher cut-off frequency of the N41 band is better than the simulated result. The group delay in the N41 band varies from 5.5 ns to 11.2 ns with 5.7 ns fluctuation while the group delay in the N79 band varies from 5.0 ns to 11.8 ns with 6.8 ns fluctuation in the passband. Notably, the group delays at the N41 and N79 bands keep 2 ns fluctuation in the 60% passband, which are contributed to the usage of the two cross-coupling lines.

**TABLE 3. Some state-of-the-art dualband Superconducting bandpass filter.**

Ref.	Freq./GHz	Bandwidth/%	Insert loss/dB	Order	Isolation/dB	Group delay	Size( $\lambda_g \times \lambda_g$ )
[9]	1.9/2.6	2.39/2.29	0.29/0.45	8	60	No	0.47×0.225
[19]	3.45/4.9	8.9/4.2	0.20/0.30	6	68	No	0.57×0.25
[20]	1.5/2.0	1.03/1.07	0.27/0.30	10	90	No	0.502×0.227
[21]	2.45/3.50	8.0/5.0	0.3/0.3	4	70	No	0.34×0.19
[22]	0.24/0.51	16.2/26.6	0.2/0.2	7	50	No	0.072×0.0625
This work	2.595/4.85	6.2/2	0.3/0.4	6	80	Yes	0.51×0.32

Table 3 shows the performance comparison between the proposed dualband filter and some state-of-the-art published works.

#### IV. CONCLUSION

A novel dualband bandpass HTS filter with group delay equalization is presented in this paper. The proposed novel DSLSIR is introduced with the merits of simultaneous control of the two required center frequencies and the corresponding coupling coefficients. The parameter study of the novel DSLSIR is accomplished as well as the resonance analysis to guide the dualband resonator design. Meanwhile, the coupling coefficient extract and the external quality factor extract method are investigated to realize the final dualband bandpass filter. Two cross-coupling lines are applied to control the group delay fluctuation at the two bands. The HTS filter is fabricated on the LaAlO<sub>3</sub> substrate and double-side YBCO films and is measured at the temperature of 77 K. The results show that the first band at 2.515-2.675 GHz is with 0.3 dB insertion loss, 20.5 dB return loss and maximal 80 dB rejection off 100 MHz of the upper sideband while the second band at 2.810-2.910 GHz is with 0.4 dB insertion loss, 10.2 dB return loss and 35 dB rejection off 40 MHz of the upper sideband. The group delays at the N41 and N79 bands keep 2 ns fluctuation in the 60% passband.

#### REFERENCES

- [1] L. Chunguang, W. Xu, W. Jia, S. Liang, and H. Yusheng, "Progress on applications of high temperature superconducting microwave filters," *Supercond. Sci. Technol.*, vol. 30, no. 7, Jul. 2017, Art. no. 073001, doi: 10.1088/1361-6668/aa69f1.
- [2] V. Singh, P. K. Ambati, S. Soni, and K. Karthik, "Enhancing satellite communications: Temperature-compensated filters and their application in satellite technology," *IEEE Microw. Mag.*, vol. 20, no. 3, pp. 46–63, Mar. 2019, doi: 10.1109/MMM.2018.2885674.
- [3] R. B. Hammond, G. L. Hey-Shipton, and G. L. Matthaie, "Designing with superconductors," *IEEE Spectr.*, vol. 30, no. 4, pp. 34–39, Apr. 1993, doi: 10.1109/6.206620.
- [4] X. Lu, B. Wei, B. Cao, X. Guo, X. Zhang, X. Song, Y. Heng, and Z. Xu, "Design of a high-order dual-band superconducting filter with controllable frequencies and bandwidths," *IEEE Trans. Appl. Supercond.*, vol. 24, no. 2, Apr. 2014, Art. no. 1500205, doi: 10.1109/TASC.2013.2290378.
- [5] H. Liu, B. Ren, X. Zhan, X. Guan, P. Wen, S. Zhu, Y. Peng, and Z. Ma, "Triband high-temperature superconducting bandpass filters using multimode resonators," *IEEE Trans. Appl. Supercond.*, vol. 26, no. 5, Aug. 2016, Art. no. 1501506, doi: 10.1109/TASC.2016.2565611.
- [6] F. Song, B. Wei, L. Zhu, Y. Feng, R. Wang, and B. Cao, "A novel tri-band superconducting filter using embedded stub-loaded resonators," *IEEE Trans. Appl. Supercond.*, vol. 26, no. 8, Dec. 2016, Art. no. 1502009, doi: 10.1109/TASC.2016.2600406.
- [7] H. Liu, J. Lei, X. Guan, L. Sun, and Y. He, "Compact triple-band high-temperature superconducting filter using multimode stub-loaded resonator for ISM, WiMAX, and WLAN applications," *IEEE Trans. Appl. Supercond.*, vol. 23, no. 6, Dec. 2013, Art. no. 1502406, doi: 10.1109/TASC.2013.2279123.
- [8] X. Guan, Y. Peng, H. Liu, J. Lei, B. Ren, F. Qin, P. Wen, F. Liu, and Y. Liu, "Compact triple-band high-temperature superconducting filter using coupled-line stepped impedance resonator," *IEEE Trans. Appl. Supercond.*, vol. 26, no. 7, Oct. 2016, Art. no. 1501905, doi: 10.1109/TASC.2016.2599919.
- [9] H. Liu, B. Ren, S. Hu, X. Guan, P. Wen, and J. Tang, "High-order dual-band superconducting bandpass filter with controllable bandwidths and multitransmission zeros," *IEEE Trans. Microw. Theory Techn.*, vol. 65, no. 10, pp. 3813–3823, Oct. 2017, doi: 10.1109/MTT.2017.2690295.
- [10] H. Liu, Y. Wang, P. Wen, and S. Zheng, "Novel tri-band high-temperature superconducting bandpass filters using asymmetric shunted-line stepped-impedance resonator (SLSIR)," *IEEE Access*, vol. 7, pp. 32504–32509, 2019, doi: 10.1109/ACCESS.2019.2900566.
- [11] J. Zhang, Q. Liu, D.-W. Zhang, and Y. Qu, "High selectivity single wide-band and quad-band HTS filters using novel quad-mode resonators with self-coupled structure," *IEEE Access*, vol. 9, pp. 103194–103203, 2021, doi: 10.1109/ACCESS.2021.3097541.
- [12] J.-S. Hong, E. P. McErlean, and B. Karyamapudi, "High-order superconducting filter with group delay equalization," in *IEEE MTT-S Int. Microw. Symp. Dig.*, Jun. 2005, pp. 1467–1470, doi: 10.1109/MWSYM.2005.1516968.
- [13] T. Yu, C. Li, F. Li, Q. Zhang, L. Sun, X. Zhang, A. He, H. Li, Q. Luo, C. Gu, H. Tian, D. Zheng, C. Gao, and Y. He, "A novel quasi-elliptic HTS filter with group-delay equalization using compact quasi-lumped element resonators in VHF band," *IEEE Trans. Appl. Supercond.*, vol. 19, no. 2, pp. 69–75, Apr. 2009, doi: 10.1109/TASC.2009.2013819.
- [14] L. Zhou, Z. Long, H. Li, T. Zhang, and M. Qiao, "A novel configuration for compact HTS CQ structure linear phase filter design," *IEEE Trans. Appl. Supercond.*, vol. 28, no. 8, Oct. 2018, Art. no. 1501608, doi: 10.1109/TASC.2018.2869796.
- [15] P. Mondal and M. K. Mandal, "Design of dual-band bandpass filters using stub-loaded open-loop resonators," *IEEE Trans. Microw. Theory Techn.*, vol. 56, no. 1, pp. 150–155, Jan. 2008, doi: 10.1109/MTT.2007.912204.
- [16] D. M. Pozar, *Microwave Engineering*. New York, NY, USA: Wiley, 2004.
- [17] J. Hong, *Microstrip Filters for RF/Microwave Applications*. New York, NY, USA: Wiley, 2011.
- [18] R. Levy, "Filters with single transmission zeros at real or imaginary frequencies," *IEEE Trans. Microw. Theory Techn.*, vol. MTT-24, no. 4, pp. 172–181, Apr. 1976, doi: 10.1109/MTT.1976.1128811.
- [19] X. Lu, X. Guo, C. Luo, B. Wei, L. Zhang, and B. Cao, "High-order dual-band superconducting filter with independently controllable passbands and wide stopband," *Int. J. RF Microw. Comput.-Aided Eng.*, vol. 28, no. 5, Jun. 2018, Art. no. e21291, doi: 10.1002/mmce.21291.
- [20] N. Sekiya, N. Kitada, K. Kishida, and T. Tsuruoka, "Compact narrow-band high-order dual-band superconducting bandpass filters using stub-loaded double-folded resonators," *Supercond. Sci. Technol.*, vol. 33, no. 9, Jul. 2020, Art. no. 095002, doi: 10.1088/1361-6668/ab9aa4.
- [21] X. Lu, X. Guo, C. Luo, B. Wei, and B. Cao, "A compact dual-band superconducting filter with fine-tuning coupling structure," *Int. J. RF Microw. Comput.-Aided Eng.*, vol. 31, no. 1, Jan. 2021, Art. no. e22477, doi: 10.1002/mmce.22477.
- [22] X. Yu, W.-B. Xi, S.-T. Wu, and P.-G. Yan, "Design of a dual-wideband high temperature superconducting filter," *Phys. C, Supercond. Appl.*, vol. 589, Oct. 2021, Art. no. 1353937, doi: 10.1016/j.physc.2021.1353937.





**KAI YANG** received the B.S. degree in electronic science and technology and the master's degree in circuits and systems from the University of Electronic Science and Technology of China (UESTC), Chengdu, China, in 1993 and 2000, respectively.

In 2001, he was promoted as an Associate Professor with UESTC, where he was promoted as a Full Professor, in 2007. In 2002, he was selected as the Academic Outstanding Young Scientist Leader Training Plan of Sichuan Province. In 2003, he was a member of the National Superconducting Standardize Technology Committee. In 2006, he was selected as a Senior Member of the Chinese Institute of Electronics (CIE). He has authored or coauthored more than 50 papers in international and domestic journals and conferences. His current research interests include high-temperature superconducting circuits and systems, and RF and microwave passive circuits.



**PENG CHEN** received the B.S. degree in electronic science and technology and the Ph.D. degree in circuits and systems from the University of Electronic Science and Technology of China (UESTC), Chengdu, China, in 2009 and 2015, respectively.

From 2015 to 2019, he was a Lecturer with the School of Aeronautics and Astronautics, UESTC. From 2017 to 2018, he was a Visiting Scholar supported by the China Scholarship Council (CSC), Tohoku University, Sendai, Japan, cooperated with Prof. Qiang Chen. Since 2019, he has been an Associate Professor with the School of Aeronautics and Astronautics, UESTC. He has authored or coauthored more than 20 papers in international journals and conferences. His current research interests include superconducting electronics, RF and microwave integrated circuits, and advanced electromagnetic communication systems.

• • •



**MINGYANG SU** was born in Shaanxi, China, in 1995. He received the B.S. degree in communication engineering from the Xi'an University of Science and Technology, Xi'an, China, in 2017, and the M.Eng. degree in electronic and communication engineering from the University of Electronic Science and Technology of China (UESTC), Chengdu, China, in 2020.

Since July 2020, he has been a Research Engineer with Tuowei Electronics Technology (Shanghai) Company Ltd., Shanghai, China. His current research interests include multilayer planar microwave filters and antennas.